Tailoring light-sound interactions in a single mode fiber for the high-power transmission or sensing applications

Aamir Gulistan, M. M. Rahman, Souvik Ghosh, and B. M. A. Rahman

City University of London

ABSTRACT

A full-vectorial numerically efficient Finite Element Method (FEM) based computer code is developed to study complex light-sound interactions in a single mode fiber (SMF). The SBS gain or SBS threshold in a fiber is highly related to the overlap between the optical and acoustic modes. For a typical SMF the acoustic-optic overlap strongly depends on the optical and acoustic mode profiles and it is observed that the acoustic mode is more confined in the core than the optical mode and reported overlap is around 94 % between these fundamental optical and acoustic modes. However, it is shown here that selective co-doping of Aluminum and Germanium in core reduces the acoustic index while keeping the optical index of the same value and thus results in increased acoustic-optic overlap of 99.7%. On the other hand, a design of acoustic anti-guide fiber for high-power transmission systems is also proposed, where the overlap between acoustic and optical modes is reduced. Here, we show that by keeping the optical properties same as a standard SMF and introducing a Boron doped 2nd layer in the cladding, a very low value of 2.7% overlap is achieved. Boron doping in cladding 2nd layer results in a high acoustic index and acoustic modes shifts in the cladding from the core, allowing much high power delivery through this SMF.

Keywords: Stimulated Brillouin Scattering, Finite Element Method, SBS Threshold, Acoustic anti-guide

1. INTRODUCTION

Light sound interaction also known as Stimulated Brillouin Scattering (SBS) in optical waveguides has attracted considerable large interest over the past years[1,2]. The SBS is a nonlinear process, when sound wave is generated due to electrostriction effect which creates a traveling Bragg gratings and prevents delivery of high optical power. Among other non-linear effects like Self Phase Modulation (SPM) or Cross Phase Modulation (XPM), the SBS has gained more attention due to the its low threshold and limiting the power scaling in the photonic devices[3,4]. However, it can also be exploited for the different applications such as distributed strain and temperature sensors[5], Brillouin cooling[6], slow and fast light[7] etc. Since early 2000's, a large number of research outputs have been reported describing reduction or increase the overlap between optical and acoustic modes for higher power transmission or for the sensing applications, respectively. These were achieved by incorporating the different materials to alter the acoustic properties of the fiber or altering the fiber dimensions. The SBS gain peaks in a Brillouin spectrum of optical fiber is highly related to the overlap between acoustic and optical modes. Dasgupta *et al.*[8], used a Finite Element Method (FEM) based commercially available software, COMSOL, to investigate the SBS spectrum in a step index Ge-doped fiber where three significant peaks were recorded in the Brillouin spectrum from 9.4 GHz to 11.6 GHz. These SBS gain peaks are the result of high overlap recorded between fundamental optical and dominant longitudinal acoustic LP_{01}, LP_{02} and LP_{03} modes. Shibata *et al.* investigated the effect of different germanium doping concentration in the core of fibers and cladding consisted of either Fluorine or pure Silica for two different fiber designs[9]. For the first design, the acoustic velocity of the cladding was taken lower than that in the core of the fiber resulting in an acoustic anti-guide design. Similarly, for second fiber design where core was doped with germanium and cladding with pure silica, waveguide acts as a acoustic guide and three peaks were reported in Brillouin spectra. Multimode fibers (MMF) have a higher effective area which results in a high SBS threshold and provides flexibility to enhance maximum transmission

Further author information: (Send correspondence to Aamir Gulistan)
Aamir Gulistan.: E-mail: aamir.gulistan@city.ac.uk

power in the fibers. Dragic *et al.* reported the existence of higher order acoustic modes in an acoustic anti-guide[10]. They reported two peaks in the Brillouin spectrum of a MMF that has a high acoustic index fluorine doped cladding. A comparison of SBS threshold between Single Mode Fiber (SMF) and MMF is demonstrated in[11]. It is demonstrated that due to large mode area of MMF, the pump power threshold is increased to 105 mW from the previously calculated 15 mW threshold power for a SMF. However, the existence of more than one modes in MMF may introduce the inter-modal interference.

An in-house full-vectorial FEM based code is developed for the optical and acoustic modal analysis in optical waveguides[12,13]. In this paper, we have proposed two designs where light sound interaction is tailored for the fiber optic sensing or high power transmission applications. As, SBS overlap is a key feature for these applications, hence, this paper mainly focus on the approaches to enhance or reduce the SBS overlap. First design where the Aluminum oxide (Al_2O_3) or Boron oxide(B_2O_3) are used to increase the SBS overlap to attain a high SBS gain. On the other hand, the second design is an acoustic anti-guide where the SBS threshold is increased by reducing the overlap between acoustic and optical modes using B_2O_3 doped high acoustic index layer in cladding.

2. MODAL SOLUTION

For our modal solution a SMF with 6.23 %wt Ge-doped core (radius=4.1 μm) and pure silica cladding is considered. The refractive indices of core and cladding are taken n_{core}= 1.44905 and c_{clad}=1.444, respectively at the operating wavelength, $\lambda = 1.55$ μm. The full-vectorial formulation for the optical modes based on the minimization of the **H**-field energy functional is used for our modal solution[14,15]. The available two-fold symmetry of the fiber is exploited in order to avoid modal degeneration and also to improve the modal accuracy with dense FEM elements in a quarter of the structure rather than distributing in the full structure. The SBS threshold where the input pump power in optical fiber becomes equals to the back reflected power is considered as a limiting factor and it varies according to relation given in Eq. 1

$$P_{th} \propto \frac{KA_{eff}\alpha_p}{G(v_{max}, L)\Gamma_{ij}} \tag{1}$$

where K is the polarization factor, A_{eff} is the optical effective area, α_p is the acoustic attenuation coefficient for the acoustic mode of order p and $G(v_{max}, L)$ is the Brillouin gain at the peak frequency for a fiber of length L[16]. The normalized overlap Γ_{ij}, between the acoustic modes and optical modes can be calculated by the Eq. 2.

$$\Gamma_{ij} = \frac{(\int |H_{im}|^2 u_{jn} dxdy)^2}{\int |H_{im}|^4 dxdy \int |u_{jn}|^2 dxdy}; \quad m, n = x, y, z \tag{2}$$

Here, H_{im} is the m^{th} magnetic field component (where, m may be x, y or z) of the i^{th} optical mode and u_{jn} is the n^{th} component of the acoustic displacement profile (where, n may be x, y or z) of the j^{th} acoustic mode[17]. From the SBS threshold equation given in Eq. 1, it is understood that the SBS threshold can be increased either by increasing the A_{eff} or reducing the acoustic-optic overlap Γ_{ij}. Figure 1 shows the contours of dominant H_y and non-dominant H_x and H_z fields of the fundamental optical LP_{01} mode. The propagation constant and effective refractive index are calculated as $\beta_{op} = 5.86205$ (rad/μm) and with that $n_{eff} = 1.4461163$, respectively.

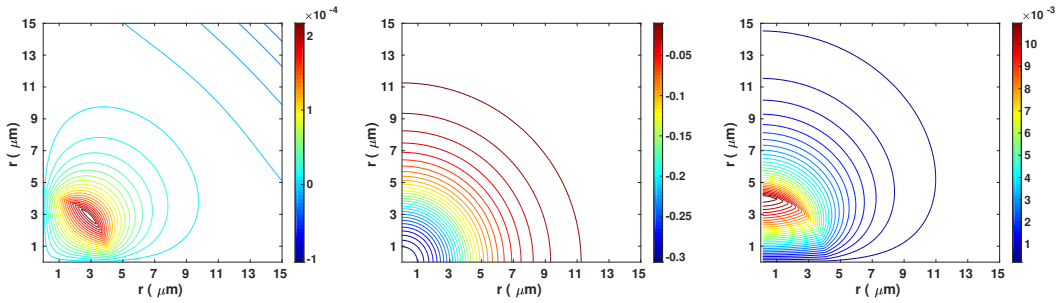

(a) (b) (b)

Figure 1: Dominant H_Y, non-dominant H_X, and H_Z field profiles of the fundamental optical mode LP_{01}, β_{op} = 5.86205 rad/μm.

Table 1: Core and cladding acoustic velocities and elastic coefficients[18].

SMF	**Materials** (%wt)		**Acoustic Velocities** (m/s)		**Density** (ρ) (kg/m^3)	**Elastic Coefficients**		
	SiO_2	GeO_2	**Shear**	**Longitudinal**		C_{11}	C_{12}	C_{44}
Core	93.76	6.24	3644.85	5794.62	2291.25	76.93488	16.05668	30.43910
Cladding	100	0	3760	5970	2201	78.44562	16.21191	31.11686

Table 1 shows the material properties of core and cladding as used for our simulations. Elastic coefficients used in stiffness matrix are derived using shear, longitudinal velocities and material density as given in Eq. 3

$$V_L = \sqrt{\frac{C_{11}}{\rho}}; \quad V_S = \sqrt{\frac{C_{44}}{\rho}}; \quad C_{11} - C_{12} = 2\,C_{44} \tag{3}$$

In order to observe light sound interaction, the following phase matching condition between optical and acoustics modes should satisfied.

$$\beta_A = 2\,\beta_{op} \tag{4}$$

Here, β_A is the wave vector of interacting acoustic mode and, β_{op} is the propagation constant of optical mode as shown Fig. 1. Figure 2 shows the dominant U_Z and non-dominant U_X and U_Y displacement vector contour plots of the fundamental longitudinal LP_{01} acoustic mode. Here, the acoustic propagation constant is calculated as β_A=11.7241 which is double of the β_{op} for the phase matching condition. The acoustic frequency and longitudinal velocity for the fundamental longitudinal LP_{01} mode are found as, f = 10.8241 GHz and V_{LG} = 5800.8286 m/s, respectively. As, SMF accommodates both longitudinal and shear modes hence, the dominant U_Y and non-dominant U_X and U_Z displacement vector are also shown in Fig. 3 for the fundamental shear mode.

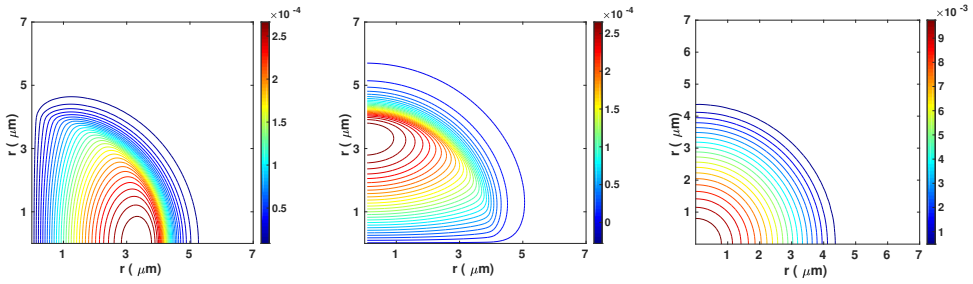

(a) (b) (b)

Figure 2: Vector displacement profiles of (a) non-dominant U_X (b) non-dominant U_Y and (c) dominant U_Z components of the fundamental longitudinal acoustic mode LP_{01} at 10.824 GHz.

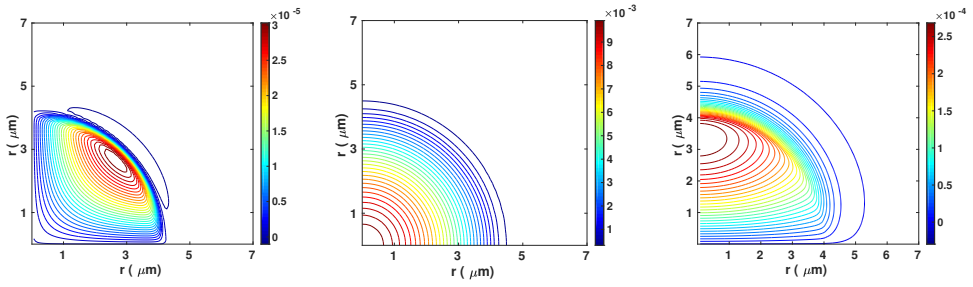

(a) (b) (b)

Figure 3: Vector displacement profiles of (a) non-dominant U_X (b) dominant U_Y and (c) non-dominant U_Z components of the fundamental shear acoustic mode LP_{01} at 6.8087 GHz.

The phase matching condition given in Eq. 4 can be satisfied by multiple acoustic modes. For example for a phase matched acoustic wave vector, fundamental and higher order modes exist that have the different frequency shift and propagation velocities. Figure 4 shows the higher order longitudinal acoustic LP_{21}, LP_{02} and LP_{03} modes. Displacement vector variation of higher order longitudinal modes along the fiber radius are also shown in the respective insets of the Fig. 4.

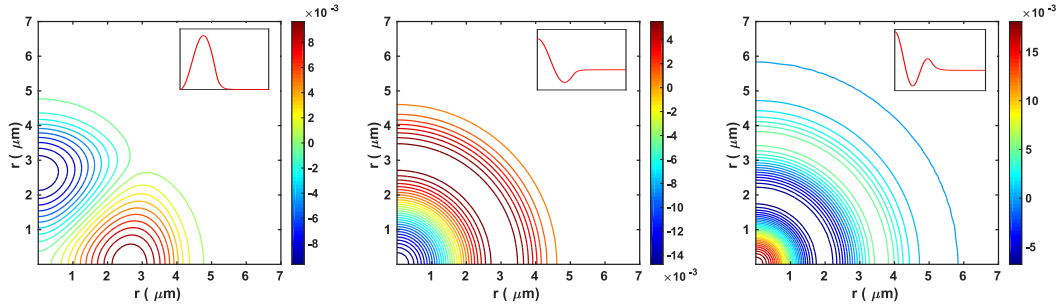

(a) (b) (c)

Figure 4: Dominant vector displacement profile U_Z of higher order phase matched longitudinal modes (a) LP_{21} (b) LP_{02} and (c) LP_{03} at 10.865 GHz, 10.873 GHz and 10.959 GHz, respectively.

Using Eq. 2 overlap values of fundamental and higher order longitudinal modes with the fundamental optical mode are calculated. As the displacement vector profile of the dominant U_Z of the longitudinal mode and dominant H_Y field of optical modes have identical nature hence, an overlap value of 94% is calculated between them. Similar, overlap has been reported in[19], where, the rectangular waveguide of similar dimensions is considered. Moreover, the overlap between the higher order (LP_{21}, LP_{02}, LP_{03}) modes and the dominant H_Y field of the fundamental optical mode are calculated as 0%, 0.91%, 0.77%, respectively. The reason for the 0% overlap between LP_{21} and optical mode is due to the odd symmetrical nature of dominant U_Z displacement vector profile of the acoustic mode. However, the overlap between non-dominant U_X and U_Y have considerable overlap due to their even symmetry and found as 35.31% and 35.233% respectively.

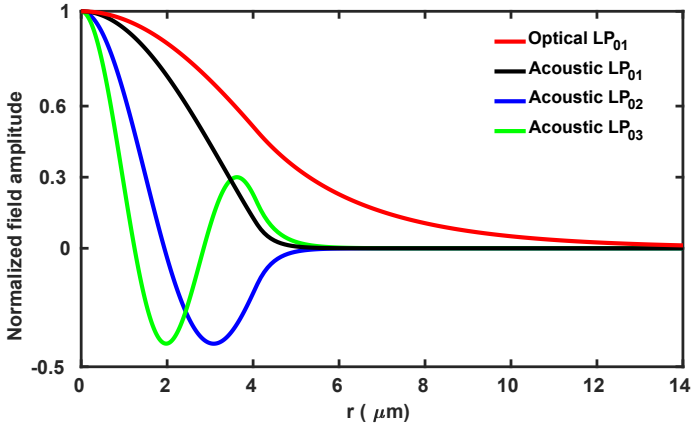

Figure 5: Normalized H_Y optical field and U_Z longitudinal displacement vector profiles along the r-axis

The normalized H_Y optical field profile of the fundamental LP_{01} optical mode, and U_Z vector profiles of the fundamental and higher order longitudinal acoustic modes along the r-axis are shown in Fig. 5. It can be observed that the fundamental longitudinal acoustic mode have the similar mode profile as of the fundamental optical mode. However, the acoustic modes are more confined in the core compared to the fundamental optical mode.

3. FIBER DESIGN FOR SENSING APPLICATIONS

3.1 Al_2O_3 doped core

Designing an acoustic co- or anti-guide is highly dependent on the choice of the doping materials. The U_Z profile for the LP_{01} acoustic mode shows it is more strongly confined than the H_Y field profile of the LP_{01} optical mode, as index contrast for the acoustic mode was higher. This index contrast can be adjusted by co-doping an optical fiber by using two or more dopants. Table 2 shows the effect of some commonly used materials for changing the optical and acoustic indices. This table shows the percentage change in the optical refractive index (Δn%), shear (ΔV_S%) and longitudinal (ΔV_L%) velocities with the percentage weight of dopant. Increase in the acoustic index results in the reduction of shear and longitudinal velocities. As discussed earlier that the acoustic modes are more confined in the core compared with the optical modes. Hence, in order to increase the optical and acoustic overlap, different %wt doping of Al_2O_3 are calculated keeping the optical refractive index n_{core}=1.44905 unchanged. This results in the less confinement of the acoustic modes in the core and thus increased overlap with the optical modes.

Table 2: Percentage weight change contribution to the optical refractive index and acoustic velocities for different dopants[20,21].

Doping material	$\frac{\Delta n\%}{Wt\%}$	$\frac{\Delta V_L\%}{Wt\%}$	$\frac{\Delta V_S\%}{Wt\%}$
GeO_2	+0.056	-0.47	-0.49
P_2O_5	+0.02	-0.31	-0.41
F	-0.31	-3.6	-3.1
TiO_2	+0.23	-0.59	-0.45
Al_2O_3	+0.063	+0.42	+0.21
B_2O_3	-0.033	-1.23	-1.18

The effect of Al_2O_3 on the fundamental acoustic mode spot-size and overlap percentage are shown in Table 3. The doping concentration of SiO_2, GeO_2 and Al_2O_3 in the core is chosen in way that the optical refractive index remain same as n_{core} = 1.44905 and only the acoustic index is modified. The shear and longitudinal velocities for the core are calculated by the relation shown in Table 2. It is observed that as the percentage of Al_2O_3 is increased the spot-size or the effective area of the fundamental longitudinal mode LP_{01} starts increasing. Overlap of 99.76% is achieved when the core is co-doped with 2.71%wt of Al_2O_3, 3.20 %wt of GeO_2 and 94.09 %wt of SiO_2.

Moreover, Table 3 also shows the effect on the spot size (σ_x) of LP_{01} as %wt of Al_2O_3 is increased further. It can be observed that as the Al_2O_3 doping is increased from 2.71%wt to higher value, the overlap start reducing as the the power start distributing on a larger effective mode area.

Table 3: Effect of Al_2O_3 doping on the core longitudinal velocity and acoustic-optic overlap

Materials (%wt)			**Fundamental Mode** LP_{01}		**Spot size** σ_x	**Acoustic-optic overlap (%)**
SiO_2	GeO_2	Al_2O_3	**Longitudinal velocity (m/s)**	**Frequency shift (GHz)**		
93.76	6.24	0	5800.8286	10.8241	3.208	94.0
93.95	4.5	1.55	5888.4942	10.9876	3.341	96.98
94.06	3.5	2.44	5938.2274	11.0804	3.546	99.16
94.09	3.2	2.71	5952.8299	11.1077	3.751	99.76
94.11	3.0	2.89	5962.2220	11.1252	4.059	98.16
94.13	2.90	2.97	5966.5666	11.1333	4.396	92.12
94.14	2.85	3.01	5968.4700	11.1369	5.087	80.56

3.2 B_2O_3 Layer in Cladding

Another technique to increase acoustic-optic overlap could be by introducing a high acoustic index layer in cladding. To achieve this a 4 μm wide annular region layer doped with B_2O_3 is used as shown as region 2 in Fig. 6. Figure 6 (a) show the schematic of the core, clad and high acoustic index 2nd layer. Whereas, Figs. 6 (b) and 6 (c) show the optical and acoustic index profiles along the radius, respectively. This high acoustic index layer in the cladding is used to reduce the confinement of the acoustic mode in the core that results in large acoustic mode area. Boron increases the acoustic index in the cladding layer resulting in the acoustic modes propagation towards cladding. The percentage weight doping of B_2O_3 is considered very carefully. If the doping percentage is increased more, the acoustic modes completely shifts in cladding that results the acoustic mode to approach its cutoff. Moreover, due to B_2O_3 doping in the cladding optical refractive index get reduced which is compensated by the addition of GeO_2 doping. The acoustic-optic overlap of 99.69% is achieved with the original core (without Al_2O_3) and high acoustic index cladding layer with doping concentration of (1.697%wt of B_2O_3 + 1%wt of GeO_2 + 97.303%wt of SiO_2).

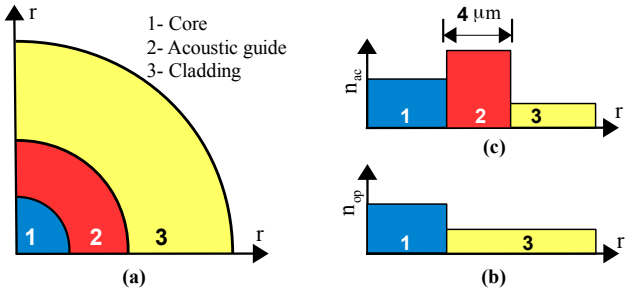

Figure 6: Effect of 2nd layer doping on the optical refractive index and the acoustic index of SMF.

4. ACOUSTIC ANTI-GUIDE: FOR HIGH POWER TRANSMISSION

As discussed in the introduction that the SBS is considered as a limiting factor in order to scale the power in the optical fiber lasers and amplifiers. Backward scattering in SBS process reduced the capabilities of the optical transmission systems by limiting maximum transmission power and introducing the high bit error rate[22]. Many techniques have been proposed in order to reduce the effect of SBS by reducing the acoustic and optical modes overlap[23–25].

Here, we have proposed a novel idea of the acoustic anti-guide that results in a very low overlap between optical and acoustic modes. The SBS threshold is highly related to the overlap between acoustic and optical modes as mentioned in Eq.2. Hence, increasing the SBS threshold results in the increased optical transmission power and improved data rate performance. For our design, we have introduced a very high acoustic index layer in the inner cladding named here as a 2nd layer as it is used for increasing overlap as discussed in Subsection 3.2. However, the difference between high overlap and reduced depends on the doping concentration of B_2O_3 in 2nd layer. Here, we have observed two cases for the doping percentage and the resultant overlap. In first case, where we kept the acoustic and optical properties of the core unchanged and only doped the 2nd layer of cladding with the (3.394%wt of B_2O_3 + 2%wt of GeO_2). The resultant overlap with the fundamental optical mode is observed to be 3.5% with the acoustic mode in 2nd layer. The acoustic mode in the 2nd layer in cladding has the frequency shift and velocity of 10.587595 GHz and 5674.08 m/s, respectively. However, it is observed that the fundamental acoustic mode in the core still exist at frequency 10.81768 GHz and having velocity 5797.3904 m/s. Figure 7 shows both the acoustic modes in the core at f=10.81768 GHz, and in the cladding at f=10.58759 GHz. With only B_2O_3 doping in the 2nd layer of cladding and without changing acoustic index in the core it was not possible to make the waveguide completely anti-guide. In order to make the core completely anti-guide, the core is also doped with the aluminum (3.061%wt of Al_2O_3 + 2.8 %wt of GeO_2) to reduce its acoustic index along with the 2nd layer doping mentioned in the first case. Here we have observed the acoustic-optic overlap of 2.7% for the dominant field of the fundamental optical and longitudinal modes.

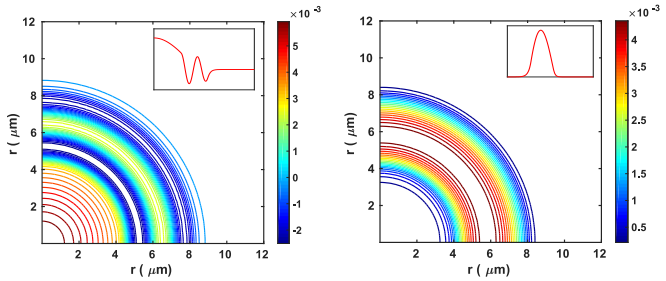

(a) (b)

Figure 7: Dominant U_Z displacement vector profile of the fundamental longitudinal LP_{01} modes (a) in the core at f=10.81768 GHz and (b) in cladding 2nd layer at f=10.58759 GHz.

Figure 8 (a) shows the contour plot of the dominant (U_Z) vector of the fundamental longitudinal mode (LP_{01}) in the proposed acoustic anti-guide design. Displacement vector profile along the radius of the fiber is also shown in inset of the Fig. 8. It can be seen that acoustic mode is shifted outside the core into cladding, however the optical modes still propagates inside the core as the optical refractive index of core and cladding were unchanged. Figures 8 (b) and (c) show the contour plots of the dominant U_Z displacement vector of LP_{02} and LP_{03} modes, respectively. Higher order longitudinal modes also shifted in the cladding resulting in a very low overlap with the optical mode.

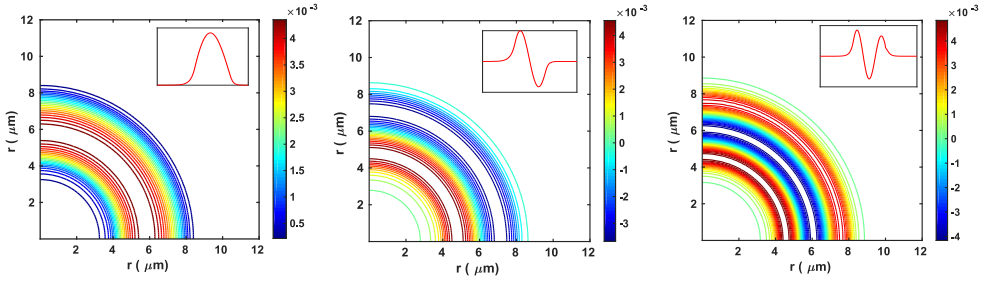

(a) (b) (c)

Figure 8: Dominant vector displacement profile U_Z of (a) fundamental longitudinal modes LP_{01} higher order modes (b) LP_{02} and (c) LP_{03} at f=10.5887 GHz, f=10.6452 GHz and f=10.7371 GHz, respectively.

Similarly, Fig. 9 shows the field profile of fundamental optical mode, and U_Z displacement vector profile of the fundamental and higher order acoustic modes along the r-axis. It can be observed that the optical mode field is confined in the core while the acoustic modes fields has shifted towards to cladding region resulting in a low overlap. Hence, the proposed design gives a high SBS threshold and it will be very useful for the long haul fiber communication, fiber lasers and amplifiers applications.

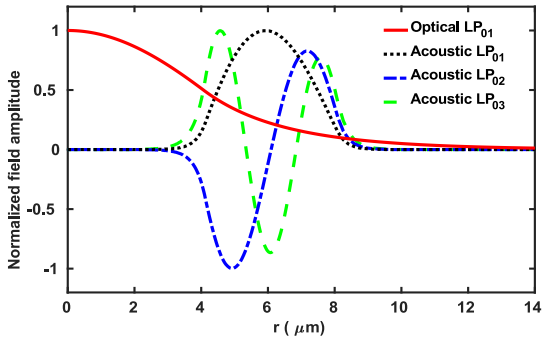

Figure 9: Normalized field and displacement vector profiles along the r-axis

5. CONCLUSION

A full-vectorial FEM is used to analyze the light-sound interaction in a SMF. Two designs are proposed, where light-sound interactions is either increased or reduced for fiber optic sensing or high power transmission applications, respectively. Acoustic-optic overlap is strongly related to the optical and acoustic mode profiles and in this case it is observed that the acoustic mode is more confined in the core than the optical mode. However, through rigorous numerical simulations, we have identified that, if the percentage (in weight) doping of Al_2O_3 (2.7%) and GeO_2 (3.2%) in the core are chosen then the core refractive index remains same as 1.44905 but its acoustic index is reduced. In this case, the acoustic mode profile become much closer to the optical mode profile and the overlap increases to 99.7%. On the other hand, an acoustic anti-guide fiber for high-power transmission systems is designed, where overlap between acoustic and optical modes is reduced. Here, we show that with the aluminum doping in the core and introducing a high acoustic index layer in the cladding (3.394% B_2O_3 +2% GeO_2) results in a very low overlap of 2.7%. This high acoustic index layer in cladding force acoustic modes to completely shifts in the cladding from the core, allowing much high SBS threshold that enables high power delivery through this SMF.

REFERENCES

[1] A. H. McCurdy, "Modeling of stimulated Brillouin scattering in optical fibers with arbitrary radial index profile." Journal of Lightwave Technology 23, no. 11, 3509, (2005).

[2] J.C Beugnot, S. Lebrun, G. Pauliat, H. Maillotte, V. Laude, and T. Sylvestre, "Brillouin light scattering from surface acoustic waves in a subwavelength-diameter optical fiber." Nature Communications 5, (2014).

[3] A. R. Chraplyvy, "Limitations on lightwave communications imposed by optical-fiber nonlinearities." Journal of Lightwave Technology 8, no. 10, 1548-1557, (1990).

[4] J. Toulouse, "Optical nonlinearities in fibers: Review, recent examples, and systems applications." Journal of Lightwave Technology 23, no. 11, 3625-3641, (2005).

[5] L. Thevenaz, M. Nikles, A. Fellay, M. Facchini and P. Robert, "Truly distributed strain and temperature sensing using embedded optical fibers, Proc. SPIE, vol. 3330, 301-314, (1998).

[6] G. Bahl, M. Tomes, F. Marquardt, and T. Carmon, "Observation of spontaneous Brillouin cooling, Nature Physics, vol. 8, pp. 203-207, (2012).

[7] K. Y. Song, K. S. Abedin, K. Hotate, M. G. Herraez, and L. Thevenaz, "Highly efficient Brillouin slow and fast light using As_2Se_3 chalcogenide fiber, Optics Express, vol. 14, no. 13, pp. 5860-5865, (2006).

[8] S. Dasgupta, F. Poletti, S. Liu, P. Petropoulos, D. J. Richardson, L. Gruner-Nielsen, and S. Herstrom, "Modeling Brillouin gain spectrum of solid and microstructured optical fibers using a finite element method," Journal of Lightwave Technology 29, no. 1, 22-30, (2011).

[9] N. Shibata, A. Yuji, T. Horiguchi, and M. Tateda, "Identification of longitudinal acoustic modes guided in the core region of a single-mode optical fiber by Brillouin gain spectra measurements." Optics letters 13, no. 7, 595-597, (1988).

[10] P. D. Dragic, C. H. Liu, G. C. Papen, and A. Galvanauskas, "Optical fiber with an acoustic guiding layer for stimulated Brillouin scattering suppression." In Conference on Lasers and Electro-Optics, Optical Society of America, (2005).

[11] V. L. Iezzi, S. Loranger, A. Harhira, R. Kashyap, M. Saad, A. Gomes, and S. Rehman, "Stimulated Brillouin scattering in multi-mode fiber for sensing applications." In fiber and optical passive components (WFOPC), 2011 7^{th} IEEE Workshop, pp. 1-4. (2011).

[12] B. M. A. Rahman, and A. Agrawal, "Finite Element Modeling Methods for Photonics." Artech House, (2013).

[13] B. M. A. Rahman, and J. B. Davies, "Finite-Element solution of integrated optical waveguides." Journal of Lightwave Technology 2, no. 5 682-688, (1984).

[14] B. M. A. Rahman, and J. B. Davies, "Waveguide solution by finite elements. IEEE Transactions on Microwave Theory and Techniques," 32(8):922928, (1984).

[15] B. M. A. Rahman, and J. B. Davies, "Finite-element analysis of optical and microwave waveguide problems." IEEE Transactions on Microwave Theory and Techniques 32, no. 1,n 20-28, (1984).

[16] M-J. Li, X. Chen, J. Wang, A. B. Ruffin, D. T. Walton, S. Li, D. A. Nolan, S. Gray, and L. A. Zenteno, "Fiber designs for reducing stimulated Brillouin scattering." In Optical Fiber Communication Conference. Optical Society of America, (2006).

[17] L. Tartara, C. Codemard, J. N. Maran, R. Cherif, and M. Zghal, "Full modal analysis of the Brillouin gain spectrum of an optical fiber." Optics Communications 282, no. 12, 2431-2436, (2009).

[18] Y. S. Mamdem, X. Pheron, F. Taillade, Y. Jaouen, R. Gabet, V. Lanticq, G. Moreau, A. Boukenter, Y. Ouerdane, S. Lesoille, and J. Bertrand, "Two-dimensional FEM analysis of Brillouin gain spectra in acoustic guiding and antiguiding single mode optical fibers." In COMSOL Conference, (2010).

[19] B. M. A. Rahman, and M. M. Rahman, "Interactions of acoustic and optical waves in Ge-doped silica planar optical waveguide." In Opto-Electronics and Applied Optics (IEM OPTRONIX), 2015 2nd International Conference on, pp. 1-4. IEEE, (2015).

[20] C. K. Jen, C. Neron, A. Shang, K. Abe, L. Bonnell, and J. Kushibiki. "Acoustic characterization of silica glasses, "Journal of the American Ceramic Society 76, no. 3, 712-716, (1993).

[21] M. J. Li, X. Chen, J. Wang, S. Gray, A. Liu, J. A. Demeritt, A. B. Ruffin, A. M. Crowley, D. T. Walton, and L. A. Zenteno, "Al/Ge co-doped large mode area fiber with high SBS threshold," Opt. Express 15, 8290-8299, (2007).

[22] F. A. Hatim, F. N. Hasoon, and S. Shaari, "Effects of nonlinear Stimulated Brillouin Scattering on performance analysis of an optical CDMA transmission system." Journal of Optical Communications 30, no. 2, 104-108, (2009).

[23] J. Nagel, V. Temyanko, M. E. Likhachev, J. Dobler, A. N. Guryanov, M. Y. Salganskii, D. S. Lipatov, M. M. Bubnov, E. M. Dianov, and N. Peyghambarian, "Experimental investigation of silicate-glass-based Raman gain fibers with enhanced SBS suppression by selective transverse doping." Journal of Lightwave Technology 34, no. 3, 928-942, (2016).

[24] M. D. Mermelstein, M. J. Andrejco, J. Fini, C. Headley, and D. J. DiGiovanni, "SBS suppression and acoustic management for high-power narrow-linewidth fiber lasers and amplifiers." In Proceedings SPIE, vol. 7580, pp. 75801G-1. (2010).

[25] S. Gray, D. T. Walton, X. Chen, J. Wang, M-J. Li, A. Liu, A. B. Ruffin, J. A. Demeritt, and L. A. Zenteno, "Optical fibers with tailored acoustic speed profiles for suppressing stimulated Brillouin scattering in high-power, single-frequency sources." IEEE Journal of Selected Topics in Quantum Electronics 15, no. 1 37-46, (2009).